

Supporting Information

Probing the Hydrogen Bonding of the Ferrous-NO Heme Center of nNOS by Pulsed Electron Paramagnetic Resonance

*Andrei V. Astashkin¹, Li Chen², Bradley O. Elmore², Deepak Kunwar², Yubin Miao², Huiying
Li³, Thomas L. Poulos³, Linda J. Roman⁴, Changjian Feng^{2,*}*

¹ Department of Chemistry and Biochemistry, University of Arizona, Tucson, AZ 85721, USA;

² College of Pharmacy, University of New Mexico, Albuquerque, NM 87131, USA;

³ Departments of Molecular Biology and Biochemistry, Chemistry, and Pharmaceutical Sciences
University of California, Irvine, Irvine, CA 92697-3900, USA.

⁴ Department of Biochemistry, University of Texas Health Science Center in San Antonio, San
Antonio, TX 78229

AUTHOR EMAIL ADDRESS: cfeng@unm.edu

CORRESPONDING AUTHOR: Changjian Feng, phone: 505-925-4326, fax: 505-925-4549.

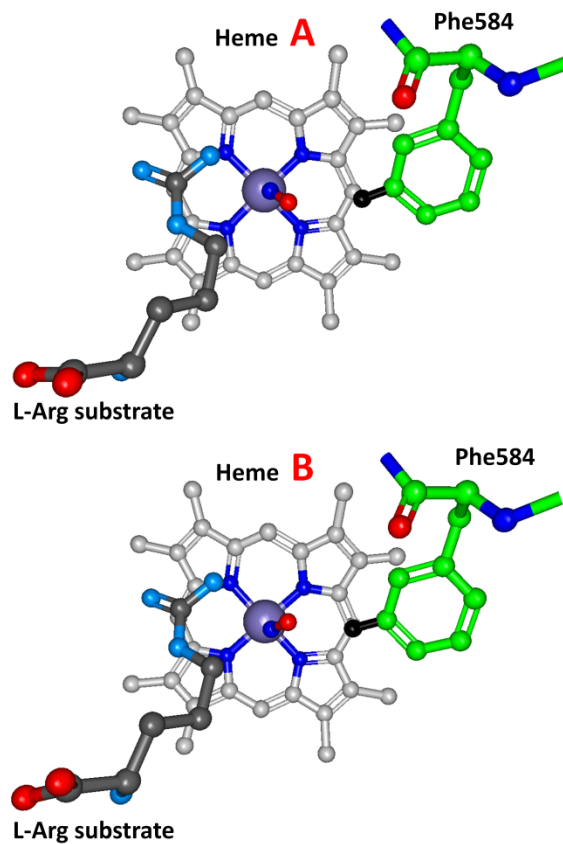


Figure S1. Selected structural elements at the two heme centers, A and B, in nNOS/Arg, as determined by X-ray crystallography (pdb 2G6K) [ref. S1]. The H_ε hydrogen of Phe584 (shown in black) is the nearest non-exchangeable hydrogen in the vicinity of the NO ligand. It at least partially eclipses one of C_{meso} carbons of the heme center, while the NO ligand rotates toward one of the neighboring pyrrol nitrogens (different for sites A and B). It is hypothesized that these NO orientations are stabilized by a weak specific interaction between O(NO) and H_ε (see main text).

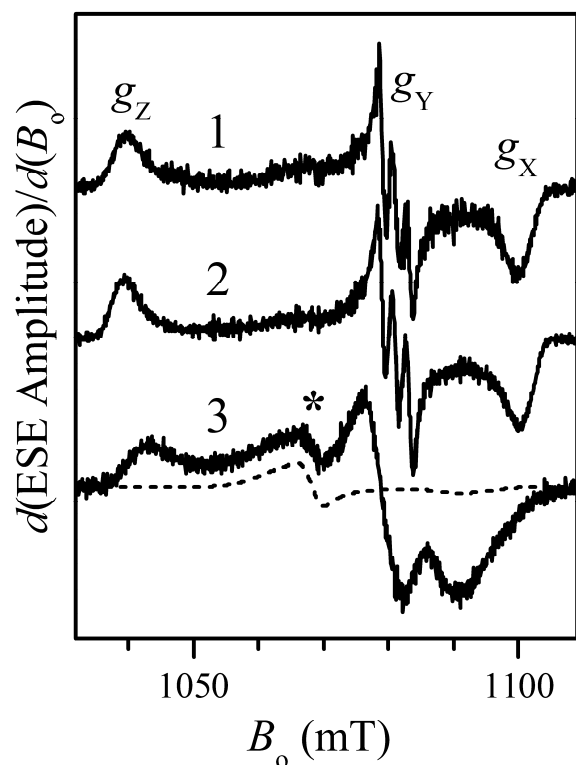


Figure S2. Numerical 1st derivatives of the two-pulse ESE field sweeps of ferrous-NO heme centers in nNOS/NS (trace 1), nNOS/Arg (trace 2), and nNOS/NOHA (trace 3). The original field sweeps are shown in Figure 2 of the main text. Experimental conditions: mw frequency, 30.305 GHz; mw pulses, 15 and 22 ns; time interval between the mw pulses, $\tau = 200$ ns; temperature, 15 K. The asterisk indicates a commonly observed feature of unknown origin. The dashed trace represents the result of the numerical simulation using $(g_1, g_2, g_3) = (2.04, 2.027, 1.982)$ and the corresponding individual linewidths of (8, 3, 8) mT (the 1st derivative of the dashed trace in Figure S3). This nearly axial spectrum is similar to the one used to explain the similar impurity in ferrous-NO myoglobin as described in [ref. S2].

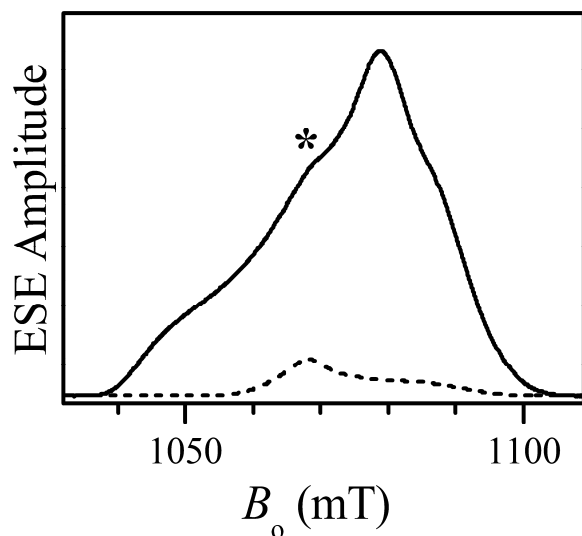


Figure S3. Solid line, the two-pulse ESE field sweep of ferrous-NO heme center in nNOS/NOHA (the same as trace 3 in Figure 2 of the main text). Experimental conditions: same as in Figure S2. The asterisk indicates a commonly observed feature of unknown origin. The dashed trace represents the result of the numerical simulation using $(g_1, g_2, g_3) = (2.04, 2.027, 1.982)$ and the corresponding individual linewidths of (8, 3, 8) mT, the 1st derivative of which is shown by the dashed trace in Figure S2. The contribution of this species to the ESE signal is $\leq 15\%$.

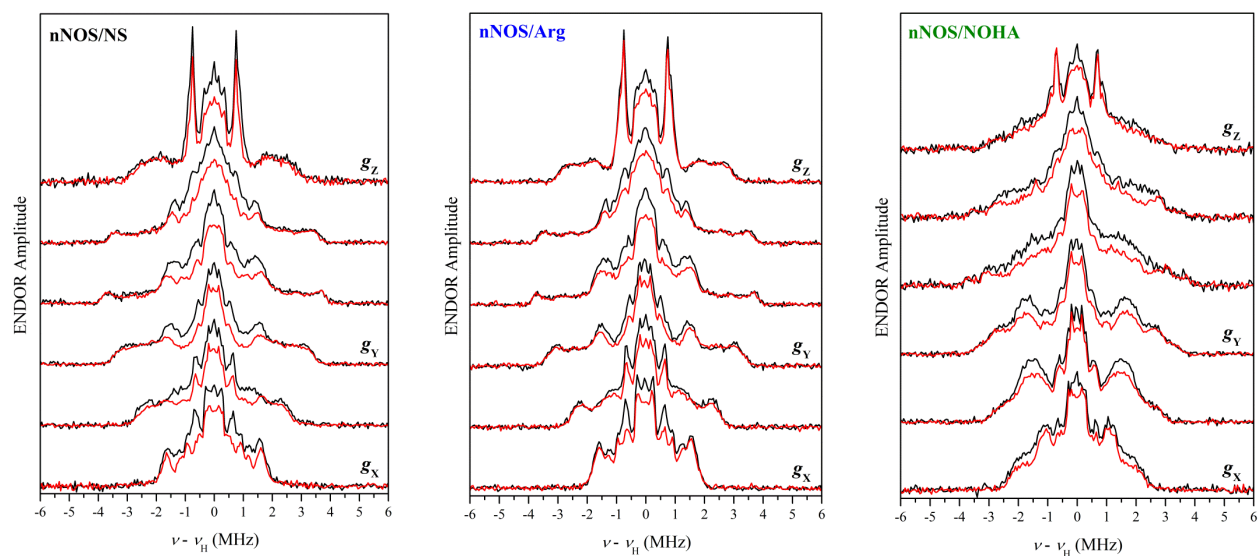


Figure S4. Refocused Mims ENDOR spectra of protons in the vicinity of ferrous-NO heme centers of nNOS/NS (left panel), nNOS/Arg (center panel) and nNOS/NOHA (right panel) in H₂O (black traces) and D₂O (red traces) recorded at the EPR positions indicated by arrows in Figure 2 of the main text. The spectra were normalized by the ESE amplitude outside any RF resonances. Experimental conditions: mw frequency, 30.305 GHz; mw pulses, 15, 15, 15, and 22 ns; time interval between the 1st and 2nd pulses, $\tau = 80$ ns; time interval between the 2nd and 3rd pulses, $T = 20$ μ s; time interval between the 3rd and 4th pulses, $t = 280$ ns; RF pulse length, 18 μ s; RF power, ~ 250 W; temperature, 15 K.

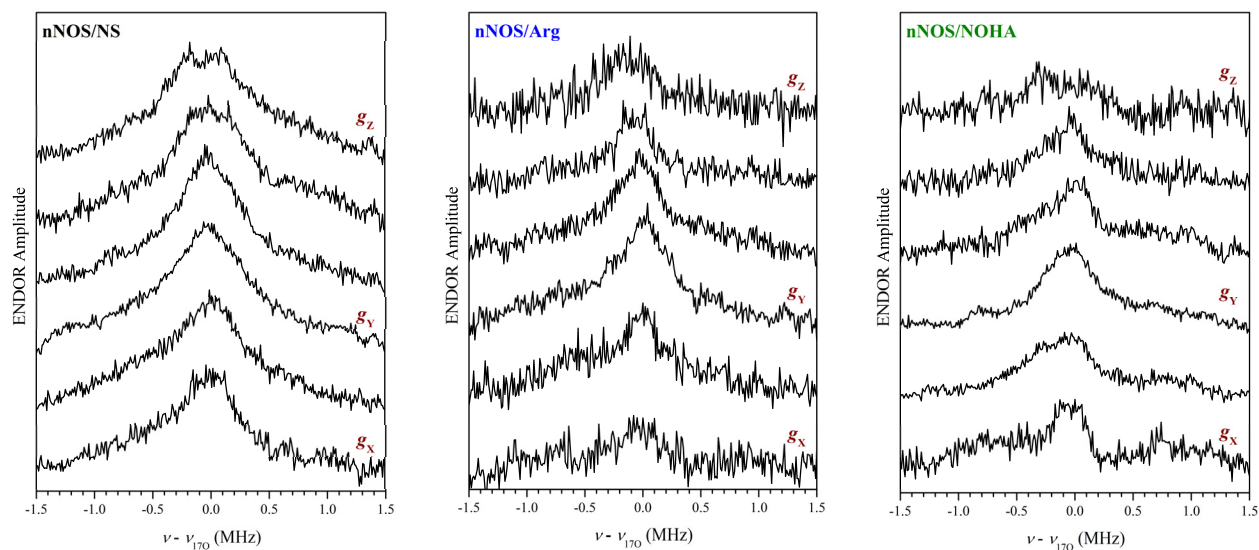


Figure S5. Mims ENDOR spectra of ^{17}O in the vicinity of ferrous-NO heme centers of nNOS/NS (left panel), nNOS/Arg (center panel) and nNOS/NOHA (right panel) in ^{17}O -enriched H_2O recorded at the EPR positions indicated by arrows in Figure 2 of the main text. The spectra were normalized by the ESE amplitude outside any RF resonances. Experimental conditions: mw frequency, 30.305 GHz; mw pulses, 15, 15, and 15 ns; time interval between the 1st and 2nd pulses, $\tau = 700$ ns; time interval between the 2nd and 3rd pulses, $T = 15$ μs ; RF pulse length, 10 μs ; RF power, ~ 800 W; temperature, 15 K.

Simulation of ^{17}O Mims ENDOR spectra. The field-integrated ^{17}O ENDOR spectra (Figure 7 of the main text and Figures S6 and S7 below) are relatively featureless, revealing mostly the central peak due to the $|-1/2\rangle \leftrightarrow |1/2\rangle$ transition of the ^{17}O spin $I = 5/2$ and a broader “bump” underneath, which is contributed to by all other transitions, but mostly the $|\pm 3/2\rangle \leftrightarrow |\pm 1/2\rangle$ ones. The $|-1/2\rangle \leftrightarrow |1/2\rangle$ transition frequency depends on the ^{17}O *nqi* to 2nd order, and the asymmetry of this line in some of the spectra is determined by this effect. All other transitions contain 1st order *nqi* contributions, and therefore the corresponding lines are much broader. The main purpose of the analysis of the ^{17}O ENDOR spectra is to estimate the anisotropic *hfi*, but the lack of well-defined spectral peaks or shoulders directly attributable to the *hfi* makes the analysis significantly more complicated than that of the ^1H ENDOR spectra (see main text).

Before considering the details of the analysis, some simplifications can be made:

- a) For the ^{17}O *nqi* we have used the known parameters determined by nuclear quadrupole resonance elsewhere [ref S3]: $e^2Qq/h \approx 6.5$ MHz, $\eta \approx 1$, where the former represents the quadrupole coupling constant and the latter is the asymmetry parameter of the *nqi* tensor (or of the tensor of the electric field gradient on the nucleus) .
- b) After preliminary simulations it became clear that the anisotropic *hfi* is weak, indicating that the ^{17}O atoms are relatively far from the NO ligand (> 3 Å). This allowed us to consider the anisotropic *hfi* tensor to be axial, characterized by a single parameter, $T_{//}$.
- c) Since the exchangeable protons were found to be beyond the H-bonding distance range, there is no mechanism for the spin density delocalization onto the water oxygen, and therefore one can take $a_{\text{iso}} = 0$.

These simplification leave us with three variable parameters: $T_{//}$ and two Euler angles, θ and ψ , describing the orientation of the *nqi* frame relative to the *hfi* one (see the Euler angle definition below; the third Euler angle, φ , is arbitrary because the *hfi* tensor is axial). The simulations thus were performed on a 3D parameter grid. The calculated well-resolved spectra were convoluted with a Gaussian broadening function, the width of which was selected to eliminate the excess resolution and make the spectra look similar to the experimental ones. The convolution width is not arbitrary: if it is too small, then the resolution is not suppressed; if it is too large, then the asymmetry of the central feature due to the 2nd order effect in *nqi* is lost.

An important experimental parameter helping to narrow down the anisotropic *hfi* values is the ratio of the normalized (by the ESE signal) amplitudes of the Mims ENDOR spectra: the amplitudes of the ^{17}O ENDOR maxima for nNOS/Arg and nNOS/NOHA are, respectively, 1.6 and 2 times smaller than that for nNOS/NS. The Mims ENDOR amplitude scaling factor ($\propto \sin^2(\pi A \tau)$, where A is the diagonal part of the *hfi* and τ is the time interval between the 1st and 2nd mw pulses) for the experimental $\tau = 700$ ns reaches the 1st maximum for $A \approx 0.71$ MHz, while our preliminary estimates give $A < 0.5$ MHz even for the spectrum of nNOS/NS, which exhibits

the broadest $|-1/2\rangle \leftrightarrow |1/2\rangle$ transition line (at half-height, $\Delta\nu \sim 0.6$ MHz). Therefore, the relative ENDOR amplitudes directly correlate with the relative T_{\parallel} values.

Some simulation examples are presented in Figures S6 and S7 below. The top three panels in Figure S6 demonstrate the sensitivity of the ^{17}O spectrum to the relative orientation of the hfi and nqi tensors; the experimental spectrum of nNOS/NS (red trace) is used for comparison. The three bottom panels in Figure S6 show simulations using the optimal (θ, ψ) of $(60^\circ, 30^\circ)$ and demonstrate the sensitivity of the simulated spectrum shape to anisotropic hfi . The central bottom panel corresponds to the optimal $T_{\parallel} = -0.36$ MHz, and the right and left bottom panels correspond to $T_{\parallel} = -0.31$ MHz and -0.41 MHz, approximately defining the error limits for the anisotropic hfi determination in this case. Thus, for ^{17}O in nNOS/NS $T_{\parallel} = -0.36 \pm 0.05$ MHz. The error limits for θ and ψ are $\pm 15^\circ$.

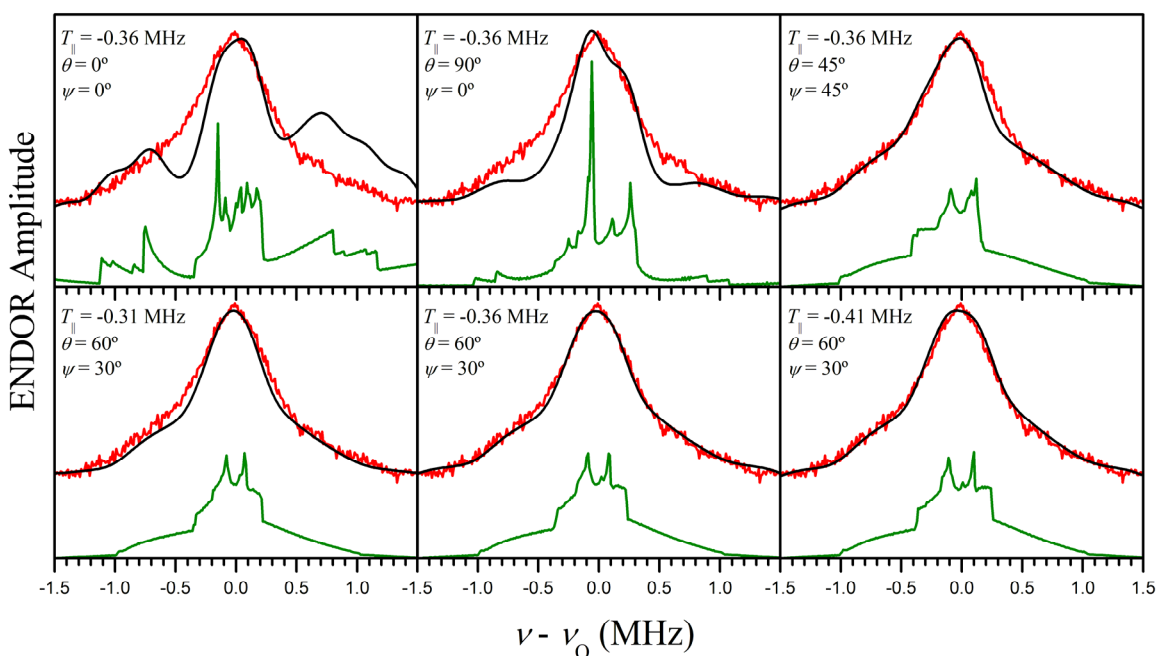


Figure S6. Red trace in each panel, field-integrated Mims ENDOR spectrum of exchangeable ^{17}O in the vicinity of ferrous-NO heme centers of nNOS/NS obtained (see main text) from the orientation-selective spectra of Figure S5. Green traces, high-resolution spectra simulated with the variable parameters shown in the panels. Black traces are obtained by convoluting the green traces with the Gaussian function with $\Delta\nu = 0.2$ MHz (between the maximum slope points). The top panels show the sensitivity of simulated spectra to θ and ψ , while the bottom panels show the sensitivity to T_{\parallel} .

The numerical simulations for nNOS/Arg show that to obtain the ENDOR amplitude 1.6 times smaller than that calculated for nNOS/NS (which would correspond to the experimental amplitude ratio), T_{\parallel} should be equal to -0.27 ± 0.03 MHz. Similar calculations for nNOS/NOHA show that to obtain the ENDOR amplitude 2 times smaller than that calculated for nNOS/NS, T_{\parallel} should be equal to -0.23 ± 0.02 MHz. Figure S7 here shows the comparison of the experimental spectra of nNOS/Arg and nNOS/NOHA with the simulations corresponding to the median T_{\parallel} values and those at the margins of the error limits. Figure 7 in the main text shows the simulations for nNOS/NS, nNOS/Arg, and nNOS/NOHA using the median $T_{\parallel} = -0.36$ MHz, -0.27 MHz, and -0.23 MHz, respectively.

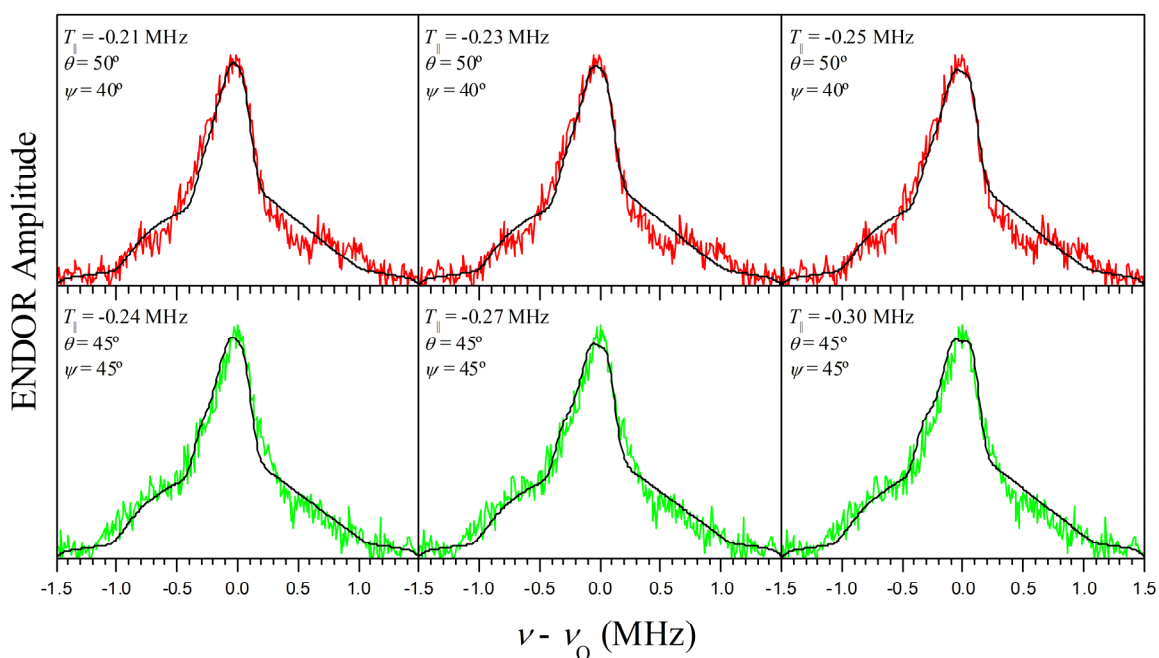


Figure S7. Comparison of the simulated ^{17}O ENDOR spectra with the experimental field-integrated Mims ENDOR spectra of exchangeable ^{17}O in the vicinity of ferrous-NO heme centers of nNOS/Arg (green traces) and nNOS/NOHA (red traces) obtained from the orientation-selective spectra of Figure S5 (see main text for the procedure). The simulations are shown by the black traces. The middle panels correspond to the median T_{\parallel} values obtained from fitting the ENDOR amplitude ratios (see above), while the left and right panels correspond to the T_{\parallel} values at the edges of the error limits defined by the amplitude ratios. The individual linewidth in the calculations was $\Delta\nu = 0.1$ MHz (Gaussian, between the maximum slope points). The angles θ and ψ are optimal, defined with the accuracy of $\pm 15^\circ$.

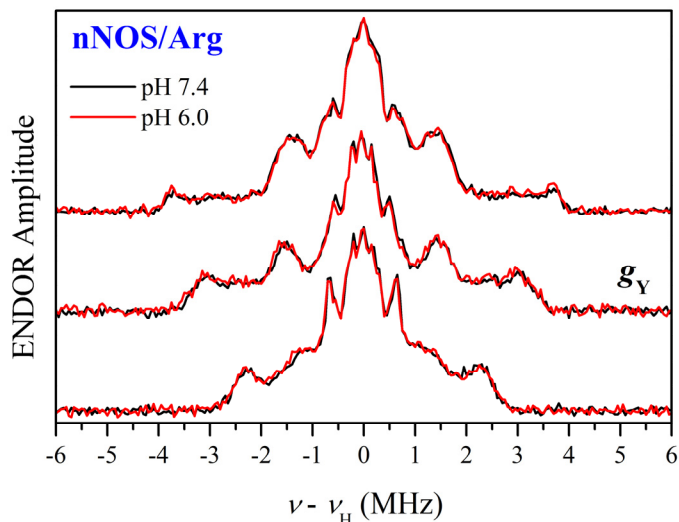
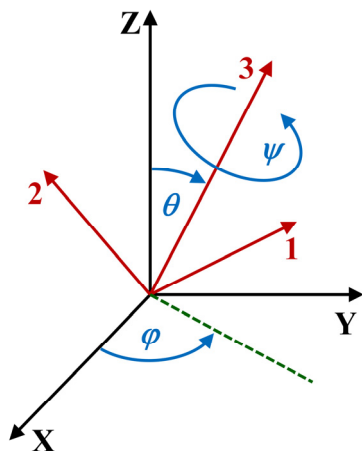


Figure S8. Refocused Mims ENDOR spectra of protons in the vicinity of ferrous-NO heme centers of nNOS/Arg in H₂O at pH 7.4 (black traces) and 6.0 (red traces) recorded at g_Y and two neighboring EPR positions out of those indicated by arrows in Figure 2 of the main text. The spectra were normalized by the ESE amplitude outside any RF resonances. Experimental conditions: same as in Figure S4.

Preparation of the ferrous-NO form of nNOS at pH 6.0. The nNOSoxy protein was concentrated and dialyzed into pH 6.0 buffer (100 mM Bis-Tris, 200 mM NaCl, 1 mM DTT, 10 μ M H₄B, 10 mM L-Arg, 10% glycerol). 300 μ L of 300 μ M nNOSoxy was added into the cuvette. The protein solution was deoxygenated by purge with dioxygen-scrubbed argon gas. NO gas was introduced into the headspace for about 15 min. The sample was then reduced with excess amount of freshly prepared dithionite solution. A \sim 40 μ L sample was transferred into a K_a-band EPR tube and rapidly frozen in a pentane and liquid nitrogen slurry.

Euler angles definition.



The Euler angles relating the coordinate frames (1,2,3) and (X,Y,Z), as used in this work, describe three consecutive rotations:

- (i) From the starting situation when the frames are aligned (1//X, 2//Y, 3//Z), rotate frame (1,2,3) around axis 3 by angle ϕ .
- (ii) Rotate frame (1,2,3) around the new axis 2 by angle θ .
- (iii) Rotate frame (1,2,3) around the new axis 3 by angle ψ .

With this definition, the polar and azimuthal angles of axis 3 in the (X,Y,Z) frame are denoted by the familiar θ and ϕ , respectively.

The angles (ϕ, θ, ψ) defined in such a way correspond to (α, β, γ) of a more standard but less easily memorizable notation.

References:

S1: Li, H. Y.; Igarashi, J.; Jamal, J.; Yang, W. P.; Poulos, T. L. Structural Studies of Constitutive Nitric Oxide Synthases with Diatomic Ligands Bound. *J. Biol. Inorg. Chem.* 11, (2006) 753-768.

S2: Radoul, M.; Sundararajan, M.; Potapov, A.; Riplinger, C.; Neese, F.; Goldfarb, D., Revisiting the Nitrosyl Complex of Myoglobin by High-Field Pulse EPR Spectroscopy and Quantum Mechanical Calculations. *PCCP* 12 (2010) 7276-7289.

S3: Edmonds, D. T.; Zussman, A. Pure Quadrupole Resonance of ^{17}O in Ice. *Phys. Lett.* 41A (1972) 167-169.